Activity enhancement of platinum oxygen-reduction electrocatalysts using ion-beam induced defects

Tetsuya Kimata,[1,2,3,*] Kenta Kakitani,[1,3] Shunya Yamamoto,[3] Iwao Shimoyama,[4] Daiju Matsumura,[5] Akihiro Iwase,[6] Wei Mao,[7] Tomohiro Kobayashi,[8] Tetsuya Yamaki,[3,†] and Takayuki Terai[1,7]

[1]*Department of Nuclear Engineering and Management, The University of Tokyo, 7-3-1 Hongo, Bunkyo-ku, Tokyo 113-8656, Japan*
[2]*Department of Materials Science and Engineering, Tokyo Institute of Technology, 4259 Nagatsuta, Midori-ku, Yokohama, Kanagawa 226-8503, Japan*
[3]*Takasaki Advanced Radiation Research Institute, National Institutes for Quantum Science and Technology, 1233 Watanuki, Takasaki, Gunma 370-1292, Japan*
[4]*Materials Sciences Research Center, Japan Atomic Energy Agency (JAEA), 2-4 Shirakata, Tokai, Ibaraki 319-1195, Japan*
[5]*Materials Sciences Research Center, Japan Atomic Energy Agency (JAEA) (SPring-8), 1-1-1 Koto, Sayo, Hyogo 679-5148, Japan*
[6]*Department of Materials Science, Osaka Prefecture University, 1-1 Gakuen-cho, Naka-ku, Sakai, Osaka 599-8531, Japan*
[7]*The Institute of Engineering Innovation, The University of Tokyo, 2-11-16 Yayoi, Bunkyo-ku, Tokyo 113-8656, Japan*
[8]*Neutron Beam Technology Team, RIKEN, 2-1 Hirosawa, Wako, Saitama 350-0198, Japan*

(Received 7 April 2018; revised 25 May 2019; accepted 16 February 2022; published 30 March 2022)

High activity is one of the primary requirements for the catalysts in proton exchange membrane fuel cell applications. Platinum (Pt) is the best known catalyst, especially for oxygen reduction at the cathode; however, further activity improvements are still required. Previous computational studies suggested that the catalytic activity of Pt nanoparticles could be enhanced by a Pt-carbon (C) support interaction. We have recently found that an enhanced electronic interaction occurs at the interface between an argon-ion (Ar^+)-irradiated glassy carbon (GC) surface and Pt nanoparticles. Here, we report a more than twofold increase in specific activity for the Pt nanoparticles on the Ar^+-irradiated GC substrate compared to that on the nonirradiated GC substrate. The mechanism of this activity enhancement was investigated by local structure analysis of the interface. Ar^+ irradiation of the carbon support led to the formation of Pt-C bonding, thus protecting the deposited Pt nanoparticles from oxidation.

DOI: 10.1103/PhysRevMaterials.6.035801

I. INTRODUCTION

The proton exchange membrane (PEM) fuel cell is a promising device that provides a highly efficient and clean source of energy. Many studies on related materials have been performed toward its widespread use [1,2]. Pt nanoparticles on a carbon material are excellent catalysts for various fuel cell reactions such as the hydrogen oxidation reaction, oxygen reduction reaction (ORR) [3], and methanol oxidation reaction; therefore, Pt is widely used in both anode and cathode electrodes in the PEM fuel cell. Potential loss at the cathode, which is caused by relatively sluggish kinetics of the ORR, is a critical issue to be solved for further improvement of the PEM fuel cell performance [4,5].

Many researchers previously proposed that the surface modification of the carbon support by thermal, chemical, or plasma treatment enhanced the catalytic activity of the Pt nanoparticles [6]. In these treatments, the particle size and dispersibility of the Pt nanoparticles were controlled by introducing surface functional groups onto the carbon supports. On the other hand, the electronic structures of the Pt nanoparticles were modulated through the orbital hybridization between Pt and C [7–9], which is termed Pt-C bonding. According to computational approaches, the formation of Pt-C bonding is increased by lattice defects of the carbon support [10], and the defective carbon support enhances the ORR activity of the Pt nanoparticles [11]. Quite recently, our experimental work revealed that ion-beam-induced lattice defects in carbon supports promote the formation of Pt-C bonding [12]. In the present study, we carried out electrochemical measurements of the Pt nanoparticles on the GC substrate irradiated with Ar^+ and then demonstrated that the Ar^+ irradiation improved their ORR activity. The mechanism of the observed activity enhancement was investigated by x-ray absorption fine structure (XAFS) measurements and density functional theory (DFT) calculations.

II. RESULTS AND DISCUSSION

The ORR activity of the Pt nanoparticles on the Ar^+-irradiated GC substrates was measured by the rotating disk electrode (RDE) method. We used the specific activity (SA), which is defined as the activity standardized by the electrochemical surface area (ECSA), of Pt within the sample. The SAs of the samples were determined by calculating i_k, the mass-transport-corrected kinetic current density. The ECSA of the electrode was calculated from

*Present address: Ground Systems Research Center, Ministry of Defense (ATLA), 2-9-54 Fuchinobe, Sagamihara 252-0206, Japan.
†yamaki.tetsuya@qst.go.jp

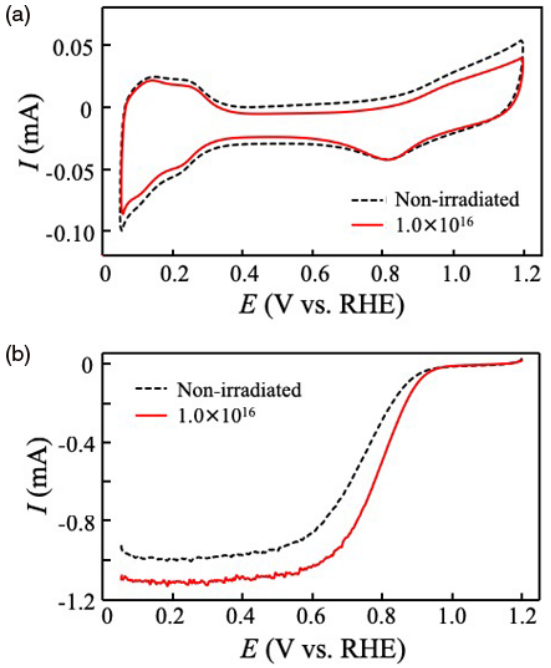

FIG. 1. Pt nanoparticles on the GC substrates irradiated with Ar ions as oxygen reduction catalysts. (a) CV curves for Pt nanoparticles on the Ar^+-irradiated GC substrates in an N_2-saturated 0.1 M $HClO_4$ solution at a scan rate of 50 mV/s. (b) ORR polarization curves for Pt nanoparticles on the Ar^+-irradiated GC substrates in an O_2-saturated 0.1 M $HClO_4$ solution at a sweep rate of 20 mV/s and a rotation rate of 1600 rpm.

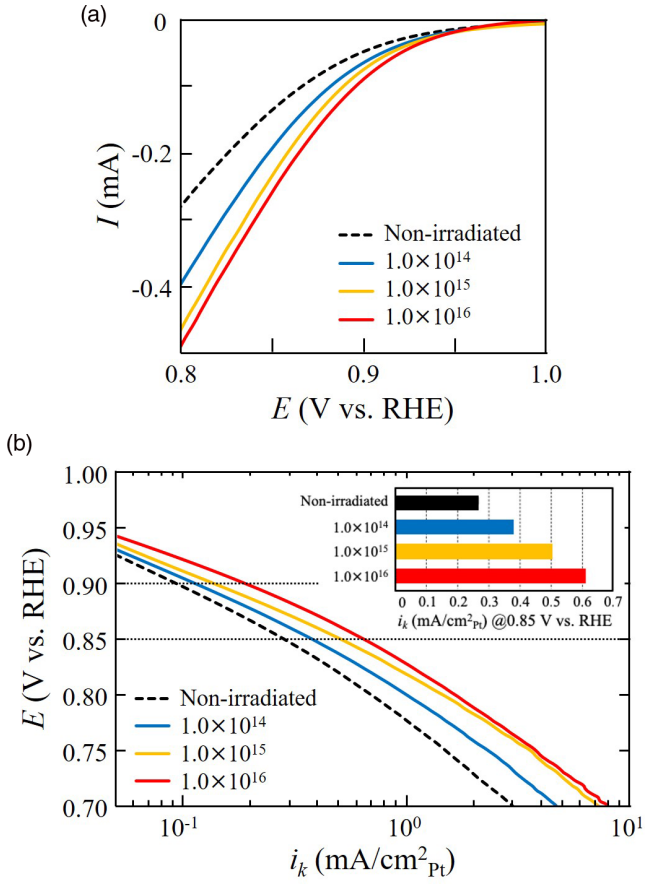

FIG. 2. ORR performance of all the samples. (a) Enlarged view of the ORR polarization curves for all the samples. (b) Tafel slopes derived from the mass-transport correction of the corresponding RDE data. Current densities are normalized to the ECSA of platinum within the samples. Inset: Current densities of all the samples at 0.85 V.

the hydrogen adsorption region during the cyclic voltammetry (CV) using a conversion factor of 210 $\mu C/cm^2$ [13]. The CV curves were compared between the Pt nanoparticles on the Ar^+-irradiated and nonirradiated GC substrates to examine how the Ar^+ irradiation affects the ECSA and the electric double layer of the samples. Figure 1(a) shows the CV curves of the Pt nanoparticles on the GC substrates in an N_2-purged 0.1 M $HClO_4$ solution. The ECSA values were estimated to be 0.59 and 0.57 cm^2 on the nonirradiated GC substrate and on the substrate irradiated at the highest fluence (1.0×10^{16} ions/cm^2), respectively. The ECSA and electric double layer of the samples did not change consistently as a function of the fluence. This can reasonably be explained by considering the change in the substrate roughness due to Ar^+ sputtering [14]. Figure 1(b) shows the linear sweep voltammetry (LSV) curves for the same samples in an O_2-saturated 0.1 M $HClO_4$ solution at a rotation rate of 1600 rpm. The ORR for all the samples was diffusion-controlled when the potential was less than 0.6 V/RHE and was under mixed diffusion-kinetics control in the potential region between 0.6 and 0.9 V/RHE.

Figure 2 shows the ORR activity of the Pt nanoparticles on the GC substrates irradiated with Ar^+ at different fluences and on the nonirradiated substrate. Figure 2(a) provides the enlarged view of the LSV curves in the range of 0.8–1.0 V/RHE for the Pt nanoparticles on the GC substrates irradiated with Ar^+ at fluences of 1.0×10^{14}, 1.0×10^{15}, and 1.0×10^{16} ions/cm^2 and on the nonirradiated GC substrate. Clearly, the ORR current of the Pt nanoparticles on the irradiated substrates began flowing at a more positive potential than their nonirradiated counterpart, and the onset potential was higher as the fluence increased. The LSV curves were recorded at four different rotation speeds, and the Koutecky-Levich plots for the ORR were straight lines. Thus, the kinetic current was derived from Koutecky-Levich theory [15], and i_k, obtained using ECSA, was represented as the Tafel slope in Fig. 2(b). The i_k at 0.90 V/RHE were 0.12, 0.14, and 0.17 mA/cm^2 for the Pt nanoparticles on the substrates irradiated at 1.0×10^{14}, 1.0×10^{15}, and 1.0×10^{16} ions/cm^2, respectively. In other words, the SA became higher with an increase in the Ar^+ fluence [Fig. 2(b) (inset)] and, at 1.0×10^{16} ions/cm^2, reached a maximum of twice that on the nonirradiated substrate (0.087 mA/cm^2). Strikingly, at 0.85 V/RHE, the maximum magnitude of the enhancement was ~2.2. These results demonstrate the enhancement of the ORR activity by the Ar^+ preirradiation of the GC.

The SA enhancement would undoubtedly be the result of the Pt-carbon support interaction at the interface. According to our recent study, the Ar^+ irradiation left the structure of the microcrystalline graphite with the largest number of vacancies and promoted the formation of the Pt-C bonding between the Pt nanoparticles and the GC substrate [12]. Therefore, the

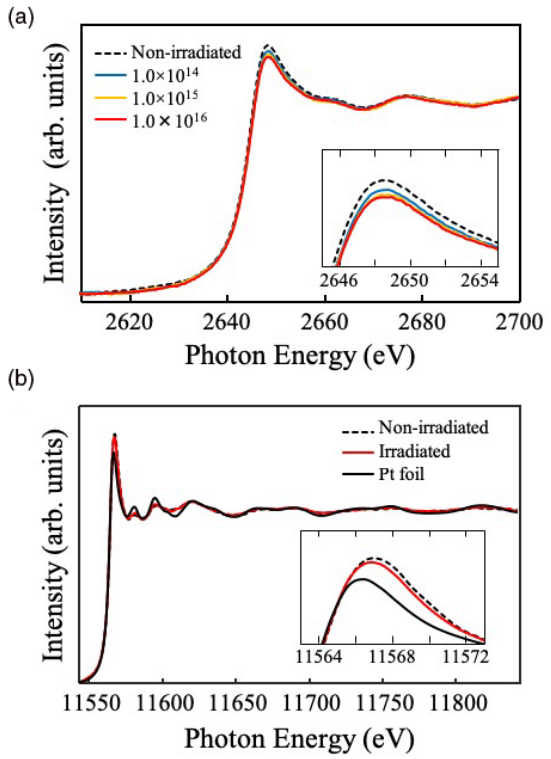

FIG. 3. XAFS spectra of Pt nanoparticles on the Ar^+-irradiated GC substrates. (a) The normalized XAFS spectra of the Pt M_3-edge measured in the TEY mode using the BL-27A of the KEK-PF. The inset shows an enlarged view of the white-line peaks. (b) The normalized XAFS spectra of the Pt L_3-edge measured in the transmission mode at the BL14B1 of SPring-8.

Pt-C bonding behavior at the interface is of great interest for obtaining an insight into the origin of the higher activity.

The interfacial structure between the Pt nanoparticles and GC substrate was investigated by XAFS measurements. We analyzed the x-ray absorption near-edge structure (XANES) data at the Pt M_3-edge and the extended x-ray absorption fine structure (EXAFS) data at the Pt L_3-edge in terms of the electronic structure of the Pt 5d band and the local bonding structure around the Pt atoms, respectively. For the XANES analysis, the x-ray absorption at the Pt M_3-edge was investigated because the Pt nanoparticles were deposited only on the surface of the samples, and a lower x-ray energy is suitable for the surface analysis.

Pt M_3-edge XANES spectra were measured in the total electron yield (TEY) mode to examine the changes in the electronic structure of the Pt 5d band. They are shown in Fig. 3(a) after normalization and background subtraction. The white-line intensity of the Pt nanoparticles was reduced on the Ar^+-irradiated substrates, and this reduction became significant as the irradiation fluence increased. These results indicate that the density of the unoccupied Pt 5d states decreased on the GC substrates irradiated with Ar^+ due to the suppression of Pt oxidation [16]. In fact, the tendency to inhibit oxygen adsorption was also observed in the LSV curve [Fig. 1(b)] [17]. In some papers about the relationship between the oxidation and ORR activity, the oxygen-containing surface layer caused slower kinetics [18,19], because desorption of O and OH would be the rate-limiting steps for the ORR at high potentials on the Pt nanoparticles [20]. Thus, we consider that the improvement of the ORR activity by the Ar^+ irradiation resulted from the suppressed oxidation.

The analysis of the EXAFS data can support the interpretation in the previous paragraph from the perspective of the local bonding structure. Figure 3(b) shows the Pt L_3-edge XAFS spectra in the transmission mode. The white-line intensity was lower, which is similar to Fig. 3(a). The radial distribution function was obtained from the EXAFS oscillation in Fig. 3(b) (Appendix B). The detailed EXAFS parameters, such as the coordination number, bond length, and Debye-Waller factor, are listed in Appendix C. This table indicates the following two important characteristics: (i) the Pt nanoparticles on the irradiated substrate exhibited a lower Pt-O coordination number than those on the nonirradiated GC surface, and (ii) the slight shortening of the Pt-Pt bond length was caused by the Ar^+ irradiation. Regarding the second characteristic, the shortened Pt-Pt bond length was reported to weaken the bond strength between O and Pt [21]. Therefore, these two findings from the EXAFS analysis are consistent with the suppressed oxidation discussed above. Note that the shorter Pt-Pt bond length would originate from the structure of the Pt/GC interface involving the Pt-C bonding.

DFT calculations were conducted to investigate the atomic structures of the irradiated GC substrates that contributed to the suppression of the Pt oxidation. The calculation models comprise a Pt_{13} cluster and three layers of graphene [10,22–26] with different vacancy configurations (Appendices A and D). Although this model does not reproduce the size of the Pt nanoparticles obtained experimentally, the same Pt clusters have been used in similar discussions in previous papers [10,22–26], and we considered that this model is applicable to the discussion of our work. After structural relaxation, the d-band center, ϵ_d [27] (average energy of the d-states), over the 13 Pt atoms for each model was calculated (Table I) [28]. Compared to the case of the pristine graphene, when the Pt_{13} cluster was supported on the multiple vacancies (defined as

TABLE I. DFT calculations. Average d-band center values of the Pt_{13} cluster on the substrates with different defective structures.

Substrate	ϵ_d of 13 atoms (eV)
Pristine graphene (PG)	−2.36
Single vacancy only in the upper layer (SV)	−2.34
Double vacancies only in the upper layer (DC)	−2.43
Single vacancies in the upper two layers (2SV)	−2.41
Double vacancies in the upper two layers (2DV)	−2.41

defective structures with more than two lattice vacancies), ϵ_d became lower by 0.05 eV or more. It is broadly accepted that ϵ_d correlates with the chemical reactivity of the Pt surface [29], and the bonding of oxygen to the Pt surface has been reported to weaken with a lower ϵ_d value [27]. Therefore, the lower ϵ_d value indicates that the multiple vacancies of the carbon support probably weaken the bonding of oxygen to the Pt clusters. Such low oxygen-adsorption ability would originate from the Pt-carbon support interaction involving the electron transfer from the Pt d-orbitals to the carbon π-sites. Thus, the suppression of the Pt oxidation can be ascribed to the Pt-C bonding between Pt atoms and the multiple vacancies of the carbon support, thereby improving the activity.

III. SUMMARY

In summary, the ORR activity of the Pt nanoparticles on the Ar^+-irradiated GC substrates increased proportionally to the Ar^+ fluence and, at 1.0×10^{16} ions/cm^2, reached a maximum of 2.2 times that on the nonirradiated one. This activity enhancement would be attributed to the Pt-carbon support interaction at the Pt/GC interface. The XAFS measurements clarified that the Ar^+ irradiation led to the suppression of the Pt oxidation. According to the DFT calculations, the lower ϵ_d value on the multiple vacancies explains the suppressed oxidation of the Pt nanoparticles, which is known to enhance the ORR activity. It follows that the formation of the Pt-C bonding promoted by the ion-beam-induced lattice defects would be the origin of the higher activity. Additionally, the ion-beam irradiation may also play an important role in durability enhancements because the Pt-carbon support interaction was reported to increase the stability of the Pt nanoparticles [6,7].

ACKNOWLEDGMENTS

The authors express their thanks to the staff of TIARA, Photon Factory, and SPring-8. The synchrotron radiation experiments were performed at the BL-27A of KEK-PF with the approval of the Photon Factory Program Advisory Committee (Proposal No. 2015G611) and at the BL14B1 of SPring-8 with the approval of the Japan Synchrotron Radiation Research Institute (JASRI) (Proposal Nos. 2015B3609, 2017B3654, 2018A3654, 2018B3654, 2019A3654, 2019B3654, 2020A3654, 2021A3654, and 2021B3654). This work was partly performed under the NIMS-RIKEN-JAEA-QST Cooperative Research Program on Quantum Beam Science and Technology. This work was supported in part by JSPS KAKENHI Grant Nos. 18H01923 and 21H04669. The authors also thank Sho Kato for his useful comments, and Yuki Fujimura and Shogo Kusano for their experimental support.

APPENDIX A: EXPERIMENTAL METHODS

1. Sample preparation

Unpolished 1-mm-thick GC substrates were obtained from Tokai Carbon Co., Ltd., Japan, and cut into 1 cm × 1 cm samples. Ar^+ irradiation was performed at an energy of 380 keV and the fluences between 1.0×10^{14} and 1.0×10^{16} ions/cm^2 using the ion implanter at the Takasaki Ion Accelerators for Advanced Radiation Application (TIARA) facility of the Takasaki Advanced Radiation Research Institute. The irradiated GC substrates were heated at 400 °C in an N_2 atmosphere for 1 h in order to remove water-related contamination. Pt nanoparticles were then deposited on this substrate by radiofrequency magnetron sputtering at room temperature. The sputtering time and the plasma output were 60 s and 20 W, respectively, for all the samples. The sample preparation method was adopted from the previous study [12].

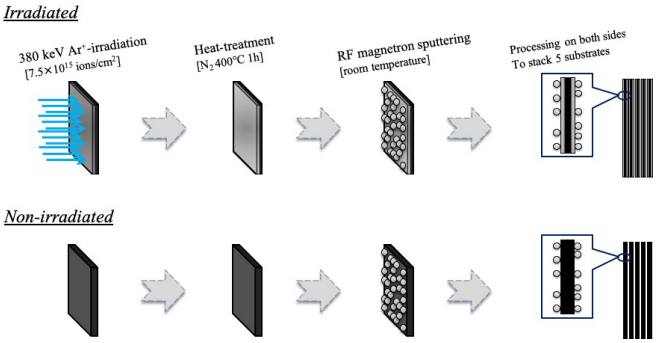

FIG. 4. Sample preparation schematic for the Pt L_3-edge XAFS measurements at SPring-8.

2. Electrochemical measurements

All the electrochemical measurements using the RDE were performed using an HZ-5000 Potentiostat (Hokuto Denko Corp., Japan), a three-electrode cell with a KCl-saturated Ag/AgCl reference electrode, and a Pt wire counter electrode. We used the experimental system from a previous study [30]. The CV measurements were performed in an N_2-saturated 0.1 M $HClO_4$ electrolyte. The electrodes were cycled in the potential range between 0.05 and 1.25 V (versus RHE) at a scan rate of 50 mV/s after electrochemical cleaning [31]. Subsequently, the LSV measurements were performed in the same potential range in an O_2-saturated 0.1 M $HClO_4$ at a scan rate of 20 mV/s with rotation speeds of 400, 900, 1600, and 2500 rpm [32].

3. XAFS measurements

The XAFS measurements of the Pt M_3-edge were carried out on the BL-27A of the Photon Factory in the High Energy Accelerator Research Organization (KEK-PF) [33] in the TEY mode to conduct surface-sensitive measurements in an ultrahigh-vacuum chamber at room temperature with a base pressure of about 1.0×10^{-7} Pa. The spectra were processed with normalization and background subtraction using the program IFEFFIT [34]. The XAFS spectra of the Pt L_3-edge were obtained at the BL14B1 of SPring-8 [35] in the transmission mode at room temperature. The samples for the Pt L_3-edge XAFS measurements were prepared as shown in Fig. 4. Fourier transformation for the EXAFS spectra and a fitting procedure were performed in the R-space with $\Delta k = 3.0$–9.5 Å^{-1} and $\Delta R = 1.3$–3.3 Å, respectively. The backward amplitude and phase shift required for the least-squares fitting of

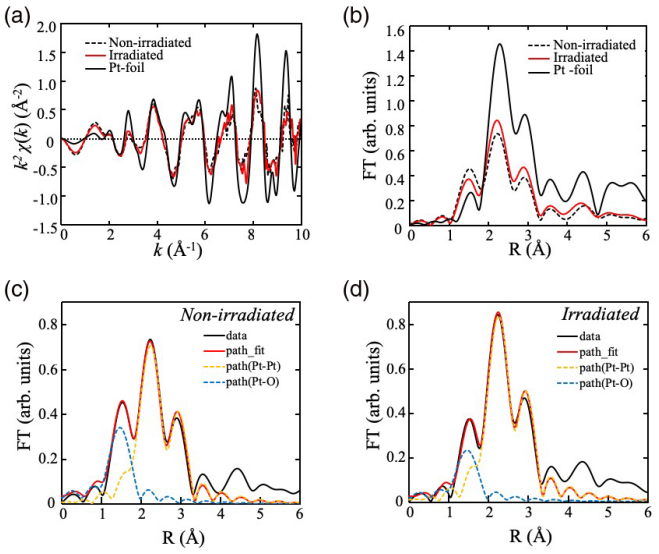

FIG. 5. (a) k^2-weighted EXAFS spectra, and (b)–(d) Fourier transform of the EXAFS spectra.

the Fourier-transformed EXAFS spectra were obtained from the FEFF 6 program [36].

4. DFT calculations

All the DFT calculations were performed using the Vienna ab initio Simulation Package (VASP). The projector augmented wave method combined with a plane-wave basis set and a cutoff energy of 400 eV was used to describe the core and valence electrons. The revised Perdew-Burke-Ernzerhof form of the generalized gradient approximation was implemented in all the calculations. A conjugate gradient algorithm was used to relax ions into their ground states. The ions were allowed to relax, but the unit cell and its shape were kept constant. The energy converge criteria were set to 10^{-4} eV for the self-consistent calculations with a γ-center $9 \times 9 \times 1$ k-mesh. To accelerate the electronic convergence, Gaussian smearing of the Fermi surface was employed with a smearing width of 0.1 eV. All of the periodic slabs had a vacuum spacing of 18 Å.

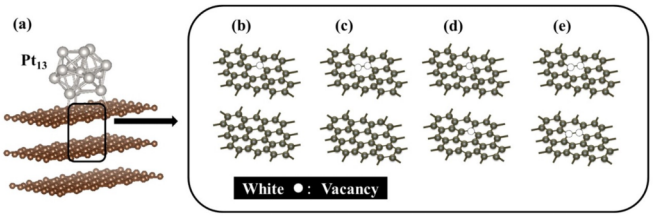

FIG. 6. (a) Calculation models of the irradiated GC and Pt nanoparticles. The interface was modeled as an icosahedral Pt_{13} cluster and three layers of graphene with (b) SV, (c) DV, (d) 2SV, and (e) 2DV.

APPENDIX B: EXAFS SPECTRA

Figure 5(a) shows k^2-weighted EXAFS spectra of the Pt-foil and the Pt nanoparticles on the GC substrate irradiated with Ar^+ at a fluence of 7.5×10^{15} ions/cm^2 and on the nonirradiated substrate. Figure 5(b) was obtained by Fourier transformation of the EXAFS spectra ($3.0 < k < 9.5$ Å^{-1}, k^2). Least-squares fitting with Pt-Pt and Pt-O nearest-neighbor coordination shells in the R space ($1.3 < R < 3.3$ Å) was treated [Figs. 5(c) and 5(d)].

APPENDIX C: STRUCTURAL PARAMETERS OBTAINED FROM THE ANALYSIS OF THE EXAFS SPECTRA

Table II shows the structural parameters obtained from the analysis of the Pt L_3-edge EXAFS spectra. In the Fourier transformation of the Pt foil, the coordination number was set to 12 as a reference. The Pt nanoparticles on the irradiated substrate exhibited a lower Pt-O coordination number than those on the nonirradiated substrate. The Pt-Pt bond length of the Pt nanoparticles on the irradiated substrate was shorter than on the nonirradiated substrate, even after errors were considered.

APPENDIX D: CALCULATION MODELS

The model of the irradiated GC and Pt nanoparticles was indicated in Fig. 6(a). The GC substrate was modeled as three layers of graphene; each layer had a 5×5 structure [25,26,37]. To simulate the irradiation defects, vacancies with different configurations [(b) single vacancy only in the upper layer (SV), (c) double vacancies only in the upper layer (DV), (d) single vacancies in the upper two layers (2SV),

TABLE II. The structural parameters obtained from the analysis of the Pt L_3-edge EXAFS spectra.

Sample	Path	Coordination number	Bond length (Å)	DW factor (Å^2)	R-factor (%)
Pt-foil	Pt-Pt	12	2.7572±0.0063	0.0031	0.0025
Nonirradiated	Pt-Pt	10.293	2.7508±0.0026	0.0088	0.0083
	Pt-O	2.041	1.9231±0.0085	0.0009	
Irradiated	Pt-Pt	10.799	2.7437±0.0031	0.0076	0.0098
	Pt-O	1.289	1.9093±0.0175	0.0003	

and (e) double vacancies in the upper two layers (2DV)] were introduced to the upper two layers. An icosahedral Pt_{13} cluster was allowed to interact with the carbon atoms [22–24]. One face of the icosahedron was in contact with the graphene, and the face center of gravity was centered at each vacancy.

[1] C. Y. Wang, Fundamental models for fuel cell engineering, Chem. Rev. **104**, 4727 (2004).

[2] R. Borup, J. Meyers, B. Pivovar, Y. S. Kim, R. Mukundan, N. Garland, D. Myers, M. Wilson, F. Garzon, D. Wood, P. Zelenay, K. More, K. Stroh, T. Zawodzinski, J. Boncella, J. E. McGrath, M. Inaba, K. Miyatake, M. Hori, K. Ota *et al.*, Scientific aspects of polymer electrolyte fuel cell durability and degradation, Chem. Rev. **107**, 3904 (2007).

[3] N. M. Marković, T. J. Schmidt, V. Stamenković, and P. N. Ross, Oxygen reduction reaction on Pt and Pt bimetallic surfaces: A selective review, Fuel Cells **1**, 105 (2001).

[4] M. K. Debe, Electrocatalyst approaches and challenges for automotive fuel cells, Nature (London) **486**, 43 (2012).

[5] D. Strmcnik, M. Escudero-Escribano, K. Kodama, V. R. Stamenkovic, A. Cuesta, and N. M. Marković, Enhanced electrocatalysis of the oxygen reduction reaction based on patterning of platinum surfaces with cyanide, Nat. Chem. **2**, 880 (2010).

[6] X. Yu and S. Ye, Recent advances in activity and durability enhancement of Pt/C catalytic cathode in PEMFC: Part II: Degradation mechanism and durability enhancement of carbon supported platinum catalyst, J. Power Sources **172**, 145 (2007).

[7] G. Gupta, D. A. Slanac, P. Kumar, J. D. Wiggings-Camacho, J. Kim, R. Ryoo, K. J. Stevenson, and K. P. Johnston, Highly stable Pt/ordered graphitic mesoporous carbon electrocatalysts for oxygen reduction, J. Phys. Chem. C **114**, 10796 (2010).

[8] E. Yoo, T. Okata, T. Akita, M. Kohyama, J. Nakamura, and I. Honma, Enhanced electrocatalytic activity of Pt subnanoclusters on graphene nanosheet surface, Nano Lett. **9**, 2255 (2009).

[9] T. Kondo, Y. Iwasaki, Y. Honma, Y. Takagi, S. Okada, and J. Nakamura, Formation of nonbonding π electronic states of graphite due to Pt-C hybridization, Phys. Rev. B **80**, 233408 (2009).

[10] I. Fampiou and A. Ramasubramaniam, Binding of Pt nanoclusters to point defects in graphene: Adsorption, morphology, and electronic structure, J. Phys. Chem. C **116**, 6543 (2012).

[11] D.-H. Lim and J. Wilcox, DFT-based study on oxygen adsorption on defective graphene-supported Pt nanoparticles, J. Phys. Chem. C **115**, 22742 (2011).

[12] T. Kimata, S. Kato, T. Yamaki, S. Yamamoto, T. Kobayashi, and T. Terai, Platinum nanoparticles on the glassy carbon surface irradiated with argon ions, Surf. Coat. Technol. **306**, 123 (2016).

[13] S. A. Sheppard, S. A. Campbell, J. R. Smith, G. W. Lloyd, T. R. Ralph, and F. C. Walsh, Electrochemical and microscopic characterisation of platinum-coated perfluorosulfonic acid (Nafion 117) materials, Analyst **123**, 1923 (1998).

[14] R. Behrisch, P. Sigmund, M. T. Robinson, H. H. Andersen, H. L. Bay, and H. E. Roosendaal, *Sputtering by Particle Bombardment I* (Springer, Berlin, Heidelberg, 1981).

[15] A. J. Bard and L. R. Faulkner, *Electrochemical Methods: Fundamentals and Applications* (Wiley, New York, 2001).

[16] Y. Yazawa, H. Yoshida, and T. Hattori, The support effect on platinum catalyst under oxidizing atmosphere: Improvement in the oxidation-resistance of platinum by the electrophilic property of support materials, Appl. Catal., A **237**, 139 (2002).

[17] T. Masuda, H. Fukumitsu, K. Fugane, H. Togashi, D. Matsumura, K. Tamura, Y. Nishihata, H. Yoshikawa, K. Kobayashi, T. Mori, and K. Uosaki, Role of cerium oxide in the enhancement of activity for the oxygen reduction reaction at Pt-CeOx nanocomposite electrocatalyst—An in situ electrochemical x-ray absorption fine structure study, J. Phys. Chem. C **116**, 10098 (2012).

[18] J. Zhang, K. Sasaki, E. Sutter, and R. R. Adzic, Stabilization of platinum oxygen-reduction electrocatalysts using gold clusters, Science **315**, 220 (2007).

[19] D.-S. Kim, C. Kim, J.-K. Kim, J.-H. Kim, H.-H. Kim, H. Lee, and Y.-T. Kim, Enhanced electrocatalytic performance due to anomalous compressive strain and superior electron retention properties of highly porous Pt nanoparticles, J. Catal. **291**, 69 (2012).

[20] J. X. Wang, J. Zhang, and R. R. Adzic, Double-trap kinetic equation for the oxygen reduction reaction on Pt(111) in acidic media, J. Phys. Chem. A **111**, 12702 (2007).

[21] P. Strasser, S. Koh, T. Anniyev, J. Greeley, K. More, C. Yu, Z. Liu, S. Kaya, D. Nordlund, H. Ogasawara, M. F. Toney, and A. Nilsson, Lattice-strain control of the activity in dealloyed core-shell fuel cell catalysts, Nat. Chem. **2**, 454 (2010).

[22] Y. Okamoto, Density-functional calculations of icosahedral M_{13} (M=Pt and Au) clusters on graphene sheets and flakes, Chem. Phys. Lett. **420**, 382 (2006).

[23] D. Higgins, M. A. Hoque, M. H. Seo, R. Wang, F. Hassan, J.-Y. Choi, M. Pritzker, A. Yu, J. Zhang, and Z. Chen, Development and simulation of sulfur-doped graphene supported platinum with exemplary and activity towards oxygen reduction, Adv. Funct. Mater. **24**, 4325 (2014).

[24] N. T. Cuong, A. Fujisawa, T. Mitani, and D. H. Chi, Effect of carbon supports on Pt nano-cluster catalyst, Comput. Mater. Sci. **44**, 163 (2008).

[25] G. Ramos-Sanchez and P. B. Balbuena, Interactions of platinum clusters with a graphite substrate, Phys. Chem. Chem. Phys. **15**, 11950 (2013).

[26] J. Ma, A. Habrioux, C. Morais, A. Lewera, W. Vogel, Y. Verde-Gómez, G. Ramos-Sanchez, P. B. Balbuena, and N. Alonso-Vante, Spectroelectrochemical probing of the strong interaction between platinum nanoparticles and graphitic domains of carbon, ACS Catal. **3**, 1940 (2013).

[27] V. Stamenkovic, B. S. Mun, K. J. Mayrhofer, P. N. Ross, N. M. Markovic, J. Rossmeisl, J. Greeley, and J. K. Nørskov, Changing the activity of electrocatalysts for oxygen reduction by tuning the surface electronic structure, Angew. Chem. **118**, 2963 (2006).

[28] K. Kakitani, T. Kimata, T. Yamaki, S. Yamamoto, T. Taguchi, T. Kobayashi, W. Mao, and T. Terai, The interface between

platinum nanoparticle catalysts and an Ar^+-irradiated carbon support, Surf. Coat. Technol. **355**, 259 (2018).

[29] B. Hammer and J. K. Nørskov, Electronic factors determining the reactivity of metal surfaces, Surf. Sci. **343**, 211 (1995).

[30] T. Hakoda, S. Yamamoto, K. Kawaguchi, T. Yamaki, T. Kobayashi, and M. Yoshikawa, Oxygen reduction activity of N-doped carbon-based films prepared by pulsed laser deposition, Appl. Surf. Sci. **257**, 1556 (2010).

[31] Fuel Cell Commercialization Conference of Japan (FCCJ), Proposals of the development targets, research and development challenges and evaluation methods concerning PEFCs, http://fccj.jp/pdf/23_01_kt.pdf.

[32] K. J. J. Mayrhofer, D. Strmcnik, B. B. Blizanac, V. Stamenkovic, M. Arenz, and N. M. Markovic, Measurement of oxygen reduction activities via the rotating disc electrode method: From Pt model surfaces to carbon-supported high surface area catalysts, Electrochim. Acta **53**, 3181 (2008).

[33] H. Konishi, A. Yokoya, H. Shiwaku, H. Motohashi, T. Makita, Y. Kashihara, S. Hashimoto, T. Harami, T. A. Sasaki, H. Maeta, H. Ohno, H. Maezawa, S. Asaoka, N. Kanaya, K. Ito, N. Usami, and K. Kobayashi, Synchrotron radiation beamline to study radioactive materials at the Photon Factory, Nucl. Instrum. Methods Phys. Res., Sect. A **372**, 322 (1996).

[34] B. Ravel and M. Newville, ATHENA, ARTEMIS, HEPHAESTUS: Data analysis for X-ray absorption spectroscopy using IFEFFIT, J. Synch. Radiat. **12**, 537 (2005).

[35] W. Utsumi, K. Funakoshi, Y. Katayama, M. Yamakata, T. Okada, and O. Shimomura, High-pressure science with a multi-anvil apparatus at SPring-8, J. Phys.: Condens. Matter **14**, 10497 (2002).

[36] J. J. Rehr and R. C. Albers, Theoretical approaches to x-ray absorption fine structure, Rev. Mod. Phys. **72**, 621 (2000).

[37] Y. Tian, Y.-J. Liu, J.-X. Zhao, and Y.-H. Ding, High stability and superior catalytic reactivity of nitrogen-doped graphene supporting Pt nanoparticles as a catalyst for the oxygen reduction reaction: a density functional theory study, RSC Adv. **5**, 34070 (2015).